Non-Equilibrium Molecular Dynamics Study of Ion Permeation through the Biological Ion Channel alpha-Hemolysin

by

William Joseph Kowallis

B.S. Chemistry, Biology, University of Pittsburgh, 2001

Submitted to the Graduate Faculty of

the College of Arts and Sciences in partial fulfillment

of the requirements for the degree of

Master of Science

University of Pittsburgh

2009

UNIVERSITY OF PITTSBURGH

School of Chemistry

This thesis was presented

by

William Joseph Kowallis

It was defended on

April 23, 2004

and approved by

Peter E. Siska, Ph. D.

Gilbert C. Walker, Professor, Ph. D.

Thesis Advisor: Rob D. Coalson, Ph. D.

Non-Equilibrium Molecular Dynamics Study of Ion Permeation through the Biological Ion Channel alpha-Hemolysin

William J. Kowallis, M.S.

University of Pittsburgh, 2009

Ion permeation properties and current-voltage (I-V) characteristics of the ion channel alpha-hemolysin (α-HL) have been calculated using non-equilibrium molecular dynamics (NEMD). In the simulation setup for our calculations, the channel was embedded in a layer of dummy atoms, which serve as an artificial membrane, and the channel structure was frozen, or held motionless throughout the simulation. This setup served to significantly reduce computational load while testing to see if realistic permeant and I-V properties for the system were maintained, by comparison to both experimental data as well as I-V data calculated using Poisson-Nernst-Planck (PNP) methodology. Additionally, diffusion constant values for both ion types inside the channel pore region were calculated using mean square displacement (MSD) methodology and compared to results for bulk solution, yielding a reduction in the diffusion constants inside the channel for each ion type of approximately one half their bulk values. While our preliminary results have produced qualitatively reasonable data, we concluded that the simulation would be more accurate if a portion of the channel structure, specifically those residues found at the protein-solvent interface, is allowed to move freely for future calculations.

TABLE OF CONTENTS

LIST OF TABLES

LIST OF FIGURES

PREFACE

I would like to thank my entire family, my friends, and my committee members and colleagues for their support and encouragement. Knowing all of you is my proudest accomplishment.

1.0 INTRODUCTION

1.1 THE IMPORTANCE OF ION CHANNEL SIMULATION STUDIES

Ion channels are essential components for proper functionality of cells and, as such, are a requirement for the existence of life. When considering cellular biology, the means by which cells are protected from the environment as well as compartmentalized within themselves is through the presence of lipid bilayers, generally being anywhere from 40 to 60 Angstroms in thickness. Considering that the amphipathic nature of these bilayers presents a barrier to the diffusion of both charged solutes and (partially) water (fig. 1), protein channels must be present to allow for the passage of such substances (fig. 2). This permeation process constitutes an essential part of cytological activities such as inter/intra-cellular signaling, metabolism, and mitosis.

With the development of microscopic-scale monitoring techniques (Neher and Sakmann, 1976), ion channels have been the subject of intensive research and experimental studies for the past 25+ years, including the development of pharmaceutical products that specifically target ion channel function (over one-third of all drugs in use and in development today, corresponding to over $2 billion in annual pharmaceutical revenues, target ion channel activity) (*Windhover's Review*, 2003). During this time, there have been numerous advances in computational approaches for the prediction of the permeant, or current-voltage, properties of these molecules

(Jordan, 1982; Jordan, 1983; Jordan 1984; Cooper et al., 1985; Levitt, 1985; Jordan, 1987; Chen, et al., 1992; Barcilon, et al., 1993; Eisenberg et al., 1995; Kurnikova et al., 1999). However, all-atom simulations of these systems, which should yield the most realistic computational data (Crozier et al., 2001 a,b), have not been feasible due to: 1.) The atomic structures of protein channels could not be resolved and 2.) All-atom, i.e. molecular dynamics, simulations have been prohibitively computationally intensive for systems of this size (tens of thousands of atoms).

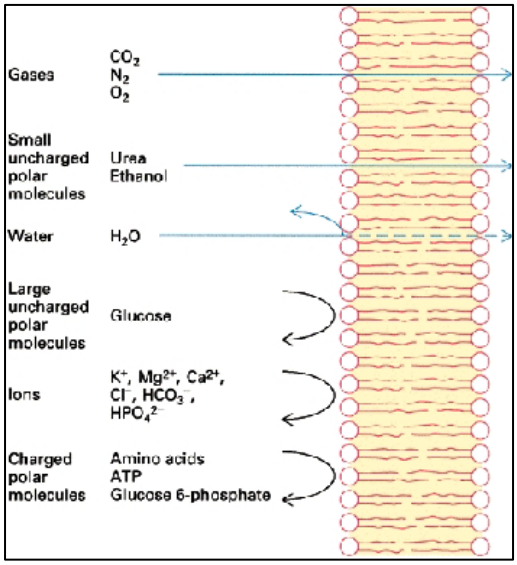

Figure 1. Diffusivities of various molecules through a phospholipid bilayer.

(http://www.mhhe.com/biosci/esp/2001_gbio/folder_structure/ce/m3/s2/)

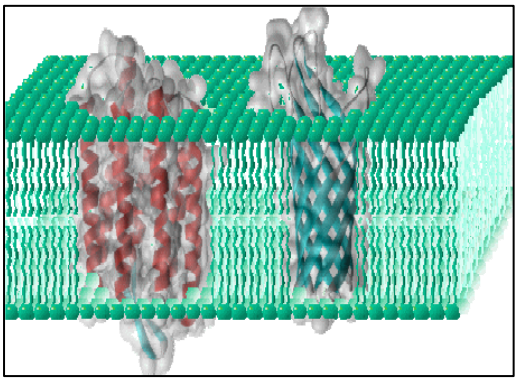

Figure 2. Examples of protein ion channels Bacteriorhodopsin (left) and OpcA (right) forming aqueous pores through a bilayer. (http://tcdb.ucsd.edu/tcdb/tcsuperfam.php?tcclass=1)

Recent developments in X-Ray crystallography (Song, et al., 1996; Doyle et al., 1998; Dutzler et al., 2002) have led to the structures of a select few channels being resolved for computational study. Further, necessary advances in computer resources, specifically at supercomputing facilities such as the Pittsburgh Supercomputing Center (www.psc.edu), presently provide the appropriate platforms for performing such large-scale computations.

We have recently performed preliminary non-equilibrium molecular dynamics (NEMD) simulations of a large ion channel, alpha-hemolysin (α-HL), where the channel is embedded in an artificial membrane, solvated in salt solution and an external voltage potential is applied across the system. These calculations were performed on the Lemieux Cluster at PSC (development grant #mcb030021p) and will be discussed in detail below. The data that we have gathered thus far has been promising, and so we are continuing these calculations to further test the applicability of using NEMD simulations to calculate ion channel current-voltage characteristics, i.e. ion permeation rates. We plan to generate a current-voltage (I-V) curve from -500mV to +500mV (at 100mV intervals) for α-HL and compare these results to both

experimental data (Misakian and Kasianowicz, 2003), as well as to corresponding results obtained in our group (Kowallis and Coalson, in preparation) using a cruder electrodiffusion model known as Poisson-Nernst-Planck (PNP) theory (Chen and Eisenberg, 1993; Kurnikova et al., 1999).

1.2 NEMD AS A METHOD FOR ION PERMEATION STUDY

Compared to other ion flux computation methods, e.g., PNP and also Brownian Dynamics (BD) simulation (Chung et. al, 1998), a molecular dynamics approach gives the highest atomic resolution. PNP treats solvated ions as well as water molecules as a continuum, thus not accounting for the atomic sizes of the ions and water. BD treats the ions as finite-sized particles and treats the water as a dielectric continuum. As such, this still does not realistically represent water solvent molecules between ions since the water molecules are not atomistically represented. For calculating ion currents in protein channels, especially in narrow pores (as suggested in Corry et al., 2000, Graph et al., 2000), explicit atomic representation with MD is the most realistic simulation approach. Since all atoms in a system are represented in MD, it is also the most computationally intensive method, and, until recent years, has not been practical.

α-HL is not a particularly narrow channel and so our PNP simulations of this system (Kowallis and Coalson, in preparation) have produced reasonably accurate results (as compared to experimental data) that can serve as a source of comparison. NEMD simulations of α-HL have not been performed yet, to our knowledge; also, an NEMD simulation of a wide channel such as α-HL should avert two significant problems commonly encountered in NEMD simulations of narrower channels. Namely, a prohibitively long sampling time needed for the

lower permeation rates in narrower channels and a need for extremely high quality (e.g., polarizable) force fields, which is further discussed below.

In NEMD calculations for ion flux through a channel, a factor to consider is the accuracy of the calculated free energy required for an ion to traverse the channel. This energy is artificially high in narrow channels, e.g. Gramicidin A (pore dia. ~4Å) (Mamonov et al., 2003), most likely due to inaccuracies in extant atomic-level force fields, including absence of delocalization/polarization across bonds and atoms. Such subtle electrostatic issues become more dominant in narrower channels where the ions are confined to a smaller volume and are thus always in close proximity to the channel structure. From the preliminary NEMD permeation data that we have gathered thus far, this effect appears to be largely diminished when the system consists of a much wider pore such as α-HL (minimum ~15Å in pore dia.).

1.3 ALPHA-HEMOLYSIN AS A MODEL SYSTEM FOR NEMD STUDY

The protein channel α-HL is secreted by *Staphylococcus aureus* as seven water- soluble monomers that bind to lipid membranes and self assemble into a heptameric channel (Gouaux, 1994; Song et al., 1996; Braha et al., 1997; Gouaux, 1998). Its open- state crystallographic structure was recently resolved (Song, et al., 1996) and its conduction properties have been studied in detail (Menestrina, 1986; Bezrukov and Kasianowicz, 1993; Kasianowicz and Bezrukov, 1995, Misakian and Kasianowicz, 2003).

Alpha-hemolysin is a good candidate for our initial foray into NEMD because it is among relatively few ion channels with a known, high-resolution structure (Song et. al, 1996). Further, current-voltage characteristics have been measured experimentally for this channel (Misakian

and Kasianowicz, 2003); these can serve as a reference point for comparison (along with PNP data). α-HL maintains a seven-fold axis of symmetry along its channel axis and consists of 2051 amino acid residues (32305 atoms). Experimental evidence shows α-HL to be anion selective and inwardly rectifying, meaning ions diffuse from extracellular (the smaller stem domain which is embedded in the membrane – see Figure 3) to intracellular (the larger, rim domain) more readily than the reverse (Misakian and Kasianowicz, 2003).

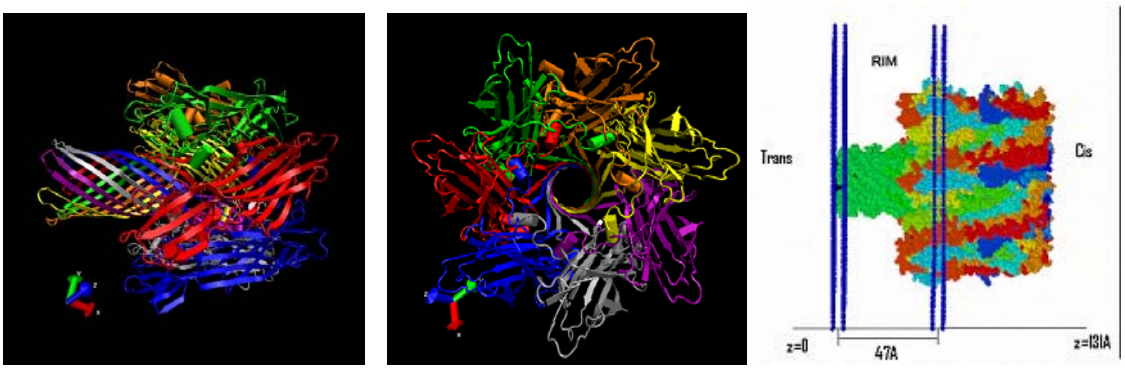

Figure 3. The left and center figures show two views of the alpha-hemolysin channel. The overall dimensions are approx. 80Å by 100Å while the pore dimensions are ~15Å in dia. by 80Å in length. The right figure schematically depicts α-HL positioned in a lipid bilayer. (Kowallis and Coalson, work in progress) [0]. [The two images w/ black background were rendered using VMD (developed by the Theoretical Biophysics Group in the Beckman Institute for Advanced Science and Technology at the University of Illinois at Urbana-Champaign) (Humphrey et al., 1996).]

2.0 COMPUTATIONAL METHODS

2.1 MOLECULAR DYNAMICS SIMULATION METHODS

Molecular Dynamics is a computational method rooted in the classical regime of physics. Modern MD techniques are an amalgam of numerous algorithms, developed over the past fifty years and designed to predict the interaction of particles in simple liquids and water (Alder and Wainwright, 1957, 1959; Rahman, 1964; Stillinger and Rahman, 1974). The first MD simulations of a protein, the bovine pancreatic trypsin inhibitor, appeared in 1977 (McCammon et al., 1977). Present MD computations have been extended to simulate realistic systems such as solvated proteins, nucleic acids, enzyme-substrate interactions, and lipid systems, e.g. biological membranes. Further, there are a variety of available software packages that perform MD computations. We chose NAMD for this study (Kale et. al, 1999) for reasons that will be discussed in the next section.

MD is a simulation technique in which the time evolution of a set of interacting particles (atoms) is determined by integrating their equations of motion. MD utilizes classical mechanical methodology, most notably Newton's Second Law: $\vec{F}_i = m_i \vec{a}_i$ for each atom in a system of N atoms, with m_i as the mass, $\vec{a}_i$ the acceleration $(d\vec{r}_i / dt^2)$, and $\vec{F}_i$ the force acting upon each

particle. This force is determined from the gradient of a potential energy function $V(\vec{R})$, $\vec{R}$ being the complete set of system coordinates (3N in all). In particular,

$$V(\vec{R}) = V_{bonded}(\vec{R}) + V_{nonbonded}(\vec{R}) \tag{1}$$

where:

$$V_{bonded}(\vec{R}) = \sum_{bonds,i} \frac{1}{2} k_i^b (r_i - r_i^o)^2 + \sum_{angles,i} \frac{1}{2} k_i^\theta (\theta_i - \theta_i^o)^2 + \sum_{torsions,i} k_i^\phi (1 + \cos(n_i \phi_i - \delta_i) \tag{2}$$

and:

$$V_{nonbonded}(\vec{R}) = \sum_{nonbondedpairs(i,j)} \{\varepsilon_{\min}^{i,j} [(\frac{r_{\min}^{ij}}{r_{ij}})^{12} - 2(\frac{r_{\min}^{ij}}{r_{ij}})^6] + \frac{q_i q_j}{\varepsilon r_{ij}}\}, \tag{3}$$

with : k_i^b = bond vibr. spring const.; r_i = bond length; r_i^o = equilib. bond length;
k_i^θ = angular spring const.; θ_i = bond angle; k_i^ϕ = torsional spring const.;
ϕ_i = rotational angle; δ = angle denoting overlap; ε = dielectric const.;
q = charge on an atom

As can be seen from equations 1-3, $V(\vec{R})$ is expressed in terms of bonded interactions plus nonbonded interactions. It is important to note here that the electrostatic contribution to the $V(\vec{R})$ expression is calculated as if the charge on each atom is a point charge at the center of mass of the atom. So, delocalization of electron density and conjugation across bonds, which are intrinsically quantum mechanical effects, are ignored in standard MD simulation. A notable exception to this is a combined QM-MD method that has been used to calculate the free energy of enzyme-substrate binding (Wymore, 2002); but to date this method is too computationally intensive to apply beyond the interactions of more than a few tens of atoms.

With both the kinetic and potential functions defined for the system, the relevant 6N dimensional Hamiltonian (3N coordinates and 3N conjugate momenta) is fully specified,

provided that the system boundaries are delimited. Knowing these system properties, the values for the potential and kinetic energies may be processed algorithmically in order to calculate the time evolution of all atoms in the system. The algorithm used in NAMD to accomplish this is the Velocity Verlet algorithm (Swope, W.C., et al., 1982), which explicitly solves for both positions and velocities:

$$\begin{aligned} r(t+\delta t) &= r(t) + v(t)\delta t + \frac{1}{2}a(t)\delta t^2 \\ v(t+\delta t) &= v(t) + \frac{1}{2}[a(t) + a(t+\delta t)]\delta t \end{aligned} \tag{4}$$

By calculating system trajectories via this algorithm, it is possible to determine the evolving microstates and thus, through kinetic sampling, determine the most probable microstates, as defined by their corresponding Boltzmann factors $e^{-\beta E_v}$, where $\beta = \frac{1}{k_B T}$ and E_v = K + V . If time evolution is sufficiently extensive, it is found that the microstate population will be distributed proportional to their corresponding Boltzmann factors. Thus, MD relies on the assumption that long time scales will provide enough sampling to yield time-averaged system properties that are equivalent in value to ensemble-averaged properties, in accordance with the Ergodic Hypothesis (Ford, 1973):

$$\langle A \rangle_{ensemble} = \langle A \rangle_{time} \tag{5}$$

At the most basic level, an MD simulation is a collection of particles in a box surrounded by vacuum, thus being isolated and forming an NVE, or microcanonical ensemble. However, this is not realistic – real systems may be contained from their surroundings, but energy exchange will still occur (e.g. thermal energy), as in the cases of NVT (canonical) and NPT (isothermal isobaric) ensembles. Of course, this coupling must be integrated into the MD

method, which is accomplished through the Nose-Hoover (for NVT) (Nose, 1984; Hoover, 1985) and Berendsen (for NTP) (Berendsen et al., 1984) algorithms, which both use Lagrange multipliers to couple the system with a constant external value of temperature or pressure. Specifically, the Nose-Hoover algorithm rescales the kinetic energies of individual particles at each time step, with the new value chosen from a range of kinetic energies averaged around a target value for the assigned temperature. The Berendsen algorithm rescales the instantaneous pressure of the system towards a target pressure value by reassigning particle positions in order to either contract or expand the system in response to a higher or lower external pressure, respectively.

Along these lines, one essential aspect for MD in determining its accuracy is choosing an appropriate time step – that is, can Δt accurately reflect the dynamics represented in the potential energy function? To illustrate this, one can consider the bond vibration energy term, i.e. the harmonic potential along a bond axis, as is given in the above description of the potential energy function. If Δt were 10 fs, then the MD time step would be longer than the period of bond vibration, thus making it impossible to represent the motion determined by this potential. As such, the time step must be short enough to ensure accurate computations and long enough to allow efficient computer usage. In order to circumvent this issue, our simulation constrains bond lengths by estimating them to a constant value by utilizing the SHAKE algorithm (van Gunsteren and Berendsen, 1977), as is utilized in NAMD.

2.2 NAMD AS A SOFTWARE PLATFORM FOR RUNNING NEMD OF α-HL

Any atomistic simulation for a system of this magnitude (>90,000 atoms) requires extensive computer resources. Therefore, it is essential to use software that is not only algorithmically sound with regard to the above mechanics of MD simulations, but is also highly parallelized, i.e., the software must be able to run simultaneously on many computers/processors without significant slowdown. Considering this, we chose NAMD software (Kale et. al, 1999), winner of the 2002 Gordon Bell award for high performance supercomputing (NAMD's high scalability was exhibited while running on PSC's TCS cluster – achieving a rating of >1Teraflop/sec on all 3000 of Lemieux's processors in Dec. 2002). According to benchmarks, NAMD has better parallel efficiency than other MD programs such as AMBER and CHARMM (http://keck2.ucsd.edu/howto/ benchmarks.html). On the Lemieux cluster, in particular, the NAMD software maintains optimal computational efficiency over a broad range of processors (http://www.ks.uiuc.edu/Research/namd/ performance.html).

Besides good parallel scalability, NAMD has other advantages, such as compatibility with AMBER and GROMACS force fields, Particle Mesh Ewald (PME) for long range electrostatic calculations, multiple time stepping for faster integration and intelligent load balancing for maximizing parallel efficiency. Continuous performance readouts are a standard feature of NAMD output files, so maintenance of high performance is easily monitored. Further, long production runs in NAMD, e.g., a 1ns, or 500,000 time step (Δt = 2fs) simulation, can be separated into 5 contiguous 100,000 time step jobs, which can be transferred via scp to one of our local hard drives without interrupting the ongoing simulations. As such, it enables us to keep the disk usage in our PSC account easily under the 10 GB quota.

2.3 HARDWARE PLATFORMS

Molecular simulation methods in general require the use of fast computing platforms; however, MD simulations of large systems (tens of thousands of atoms) such as α-HL, for a time interval of 10's -100's of nanoseconds range, require the use of computational power that can only be attained through use of a supercomputer, e.g. the Lemieux Cluster at the Pittsburgh Supercomputing Center, over the course of several months. Smaller systems, such as our local computing cluster, are still useful for simulation setup and initial equilibration calculations. Considering the importance of computing resources for successful simulations, it is essential to be able to determine the performance specs of any platform whose use is being contemplated.

2.3.1 Local Cluster

Our current local hardware capability includes a fourteen-node Dual Athlon (1.6GHz processor) Linux cluster that is interconnected by a 100 Mbps switch. We used this cluster for system setup, energy minimization, benchmarking, and short equilibration trajectories. From previous experience with a smaller system (ca. 5000 atoms), each MD step is executed quickly on individual nodes, but generation of a 10-20 ns trajectory required for the generation of an I-V point is exceedingly slow (17 days for one node to run 1 ns). Network communication among the nodes is carried out relatively slowly due to high latency and low bandwidth of the cluster interconnection network (as compared to the Lemieux cluster), i.e. the computers cannot exchange data with each other at a rate that matches their own computations. This results in limited communication rates between nodes and thus low parallel computing ability. The speedup achieved on our cluster is optimal with four processors (×2.1), after which there is no

increase in parallel performance – for this simulation setup running on all fourteen nodes the slowdown is approximately 50%. Such observations are further supported by the fact that large systems like α-HL (50,000 mobile atoms – mostly solvent and ions - in benchmark runs), where the calculations at each time step are much more lengthy and so the nodes are not continuously exchanging information (as would be the case for rapid time steps) scale much better on our cluster than do systems in the range of 5,000 atoms (e.g. Gramicidin A). Even considering these scaling issues, the overall computing power available on our cluster is not sufficient to carry out the calculations required in this study.

2.3.2 Lemieux Cluster (TCS) at Pittsburgh Supercomputing Center

Considering that NAMD performance benchmark calculations done on the Lemieux Cluster, also called the Terascale Computing System (TCS), (http://www.ks.uiuc.edu/Research/NAMD/performance.html) reveal very high efficiency of parallel calculations and that this high parallel efficiency (~100%) is maintained on 32 nodes (128 processors), then taking advantage of the TCS Quadrics architecture should be expedient for carrying out our simulation. Assuming the above are efficiencies to be maintained, optimally it will take ca. 1 day to perform 2.7 ns of simulation (three 0.9ns jobs at 8hrs computer time each) on 128 processors on the TCS platform at PSC.

As such, our longer equilibration runs (totaling 2ns simulation time) as well as all production runs to date have been carried out on the Lemieux (TCS) cluster at the Pittsburgh Supercomputing Center. Features of the Lemieux cluster that are essential for efficient computations for our α-HL system include that the TCS platform is comprised of 750 nodes, each with four 1GHz alpha processors and 4GB memory. They are interconnected through a

quadrics interconnection network that allows >1GB/sec data transfer rate between nodes, yielding a computing platform that is highly efficient for running programs in parallel.

Further, the queue system (an electronic registry that submits jobs to the cluster, based upon order of submission as well as various rankings of preference with regards to job size) at PSC allows for the submission of contiguous jobs; i.e. it is possible to include in a job submission code a command that, upon the completion of the present job, automatically loads the final coordinates and velocities from the output trajectories into a new job that will use these as the starting point for its simulation.

3.0 MOLECULAR DYNAMICS SIMULATION METHODS

3.1 EMBEDDING α-HL STRUCTURE IN MEMBRANE

The first step in preparing α-HL for simulation setup was to embed the protein channel in a layer of fixed Lennard-Jones (L-J) spheres (uncharged, non-interacting particles) (Fig. 5), also termed dummy atoms here, that provide an impermeable barrier to the passage of waters and ions, and so represent the lipid bilayer. The use of dummy atoms in place of a realistic bilayer is done in order to reduce to overall number of interacting atoms in the system and thus significantly reduce computational load, as is discussed further in section **6.1**. The x-ray crystallographic structure of α-HL was downloaded from the Research Collaboratory for Structural Bioinformatics Data Bank, also known as the Protein Data Bank (Berbstein et al., 1977), ID # 7AHL (Song et al., 1996). Missing hydrogen atoms, which are not resolved in x-ray crystallographic methods, were added to the structure using XPLOR (Brünger, 1992), water molecules that were resolved as part of the x-ray structure removed, and the channel structure was repositioned so that the pore axis was oriented normal to the x-y plane (the plane of the bilayer), which is the proposed position of α-HL in the bilayer (Song et al., 1996).

The structure was then placed in a water box of dimensions 110Åx110Åx92Å using the program SOLVATE (Grubmüller, 1996), with these dimensions chosen as to completely encompass the structure along the sides, yet leaving approx. 5Å of the channel extending beyond

the solvation box in either z direction (see fig. 4 for a side view of the channel embedded in the dummy atoms). This allows for the channel structure to electrostatically interact with ions in solution on either side of this artificial membrane. Waters were then cut from the pore cylinder and the solvation box itself was cut normal to the xy plane into a hexagonal shape of dimensions 96Å x 96Å x96Å – just wide enough to encompass all of the heptameric structure. A hexagonal system shape is required in NAMD to allow periodic boundary conditions, allowing for increased accuracy in electrostatics calculations via multi-particle Ewald sums as well as for proper flow of ions, discussed below. The last step was to then select all of the waters that remained, all of which surrounded the external sides of the α-HL structure (Fig. 4), and first remove their hydrogens and then strip their charges, thus effectively converting them into L-J spheres (Fig. 4).

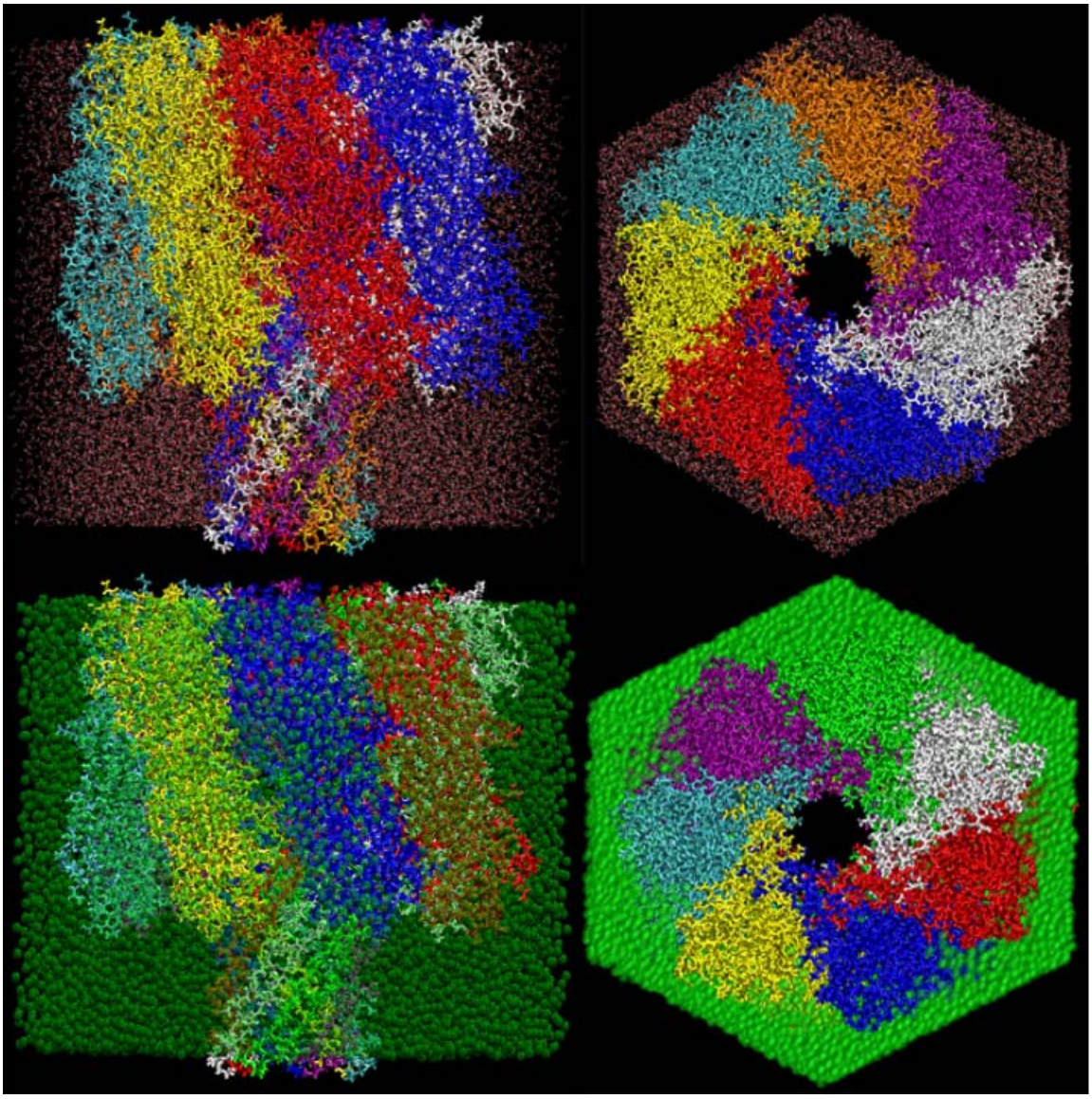

Figure 4. Views of the initial embedding of α-HL in a layer of dummy atoms. The two top figures are of initial solvation and then, as shown in the bottom two pictures, the conversion of the waters into L-J spheres. Note that ~5Å of the channel structure protrudes from the "membrane" at either end. [Pictures made with VMD (Humphrey et al., 1996)]

The system was then again solvated in a water box of dimensions 110Åx110Åx 140Å, so that the water would extend approximately 20Å beyond the end of the channel structure. This

water box was then cut hexagonally in the same fashion as before, except this time water molecules were not removed from inside the pore cylinder. Sodium and chloride ions were placed into the solution in order to bring the ionic concentration to 1M, NaCl, with the qualification that seven more Cl- than Na+ ions were added (297 Cl- + 290 Na+ = 587 total ions) in order to bring the overall system to a charge neutral state (α-HL has a +7 overall charge as a sum of partial and ionic charges in its crystal structure) (Fig. 5).

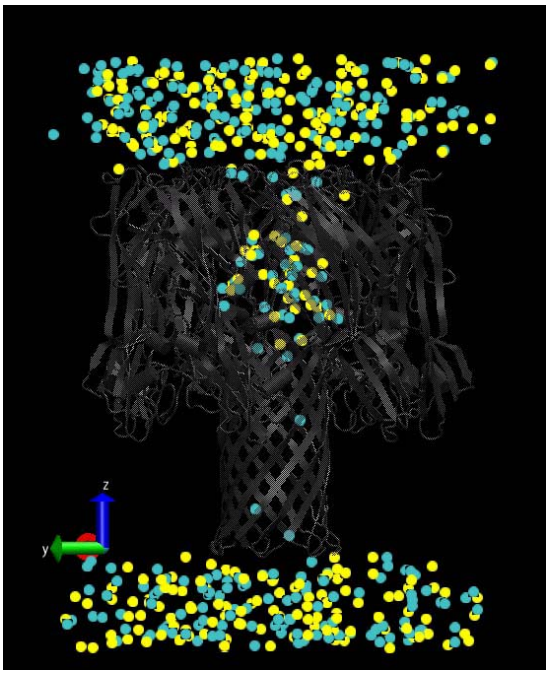

Figure 5. NEMD simulation setup: α-HL has been solvated in 1M NaCl and embedded in L-J spheres (not shown) that form an effective barrier to solvent penetration over the length of the channel (w/ axes shown). Chloride and sodium ions appear as blue and yellow spheres, respectively; waters are not shown. (Kowallis and Coalson, work in progress) [0]

3.2 EQUILIBRATION

After the dummy layer formation and solvation, the system was equilibrated as an NPT ensemble at 298K (the temperature used during the Kasianowicz experimental study) with an applied pressure of 1 atmosphere along the z-axis. For this process, both the channel structure and the L-J spheres were held fixed, periodic boundary conditions disabled, and the time step was set to 2fs. The system was allowed to relax in the z-dimension while the x-y area remained fixed (the cell volume remains fixed during production runs). This allowed for the system to compress like a piston – where waters diffused into the channel pore, filling spaces that were not effectively solvated by SOLVATE, while the outside water layer compressed accordingly. (SOLVATE was set to insert water molecules into the channel at low density, no closer than 2Å from any other atom in order to insure that waters were not inserted into small open spaces inside the protein structure)

After 1ns of equilibration, it was noted that water molecules inside the pore were migrating into spaces along the surface of channel structure in order to occupy spaces that were not effectively filled by SOLVATE, leaving empty spaces inside of the channel. Instead of waiting for waters to migrate in to fill these spaces from outside of the channel, the pore area was resolvated and equilibrated for another 2ns, after which no empty spaces appeared in the pore. After equilibration, the system dimensions were 96Å by 96Å by 128Å (note the reduction in the z- coordinate from 140Å – a result of the NTP equilibration).

3.3 PRODUCTION RUNS

For the generation of current-voltage curves, the system temperature was fixed at 298K. The dimensions of the cell were set to constant values, making it an NVT ensemble, and periodic boundaries were set in all three dimensions, thus allowing for ions to recycle instead of simply collecting at opposite sides of the system, as would be the result with an applied voltage and no periodic boundary conditions. Voltage was applied via an embedded function in NAMD in which the required voltage bias was converted to units of calories/electron charge (e_o) and divided by the overall length of the simulation system in the z-direction (128Å), since the voltage is applied across the membrane, thus yielding an electric field in units of cal./e_o-Å (a potential of +200 mV across the 128Å simulation system corresponds to an electric field of +.036 cal./e_o-Å). The time step for production runs at +1V applied potential was 2fs for the first 4ns of simulation and then was changed to 3fs in order to compare permeation statistics as well as to test if the simulation system would remain stable (which it did). The CHARMM27 parameter set (Schlenkrich et al., 1996; MacKerell Jr. et al., 1998; Feller and MacKerell, 2000) was used for all simulations. The particle mesh Ewald method (Darden et al., 1993) was used for computation of electrostatic forces without truncation. The Berendsen and Nose-Hoover algorithms were used to maintain a constant pressure of 1 atm (during equilibration) and a constant temperature of 298 K (as mentioned), respectively (Feller et al., 1995).

To efficiently simulate this system in our current calculations, our plan is to freeze the structure of the protein channel except for those residues that line the channel surface (Fig. 6). This means that atomic fluctuations for most of this molecule will not be considered and that interatomic forces within the fixed α-HL structure will not be calculated, thus reducing the required computation power. During initial simulations in our development grant at PSC

(#mcb030021p), the entire protein structure (~23,000 atoms) was held frozen to minimize the computation time needed to produce results that tested the accuracy and applicability of this approach. Performing further simulations in which the residues lining the interior surface of the channel structure are free to move will add increased realism to the model, discussed further in section **6.2**. Since most of the protein and all dummy atoms are frozen in our simulation, the only atoms that affect the computation are the solvent and the mobile ions, which consists of approximately 50,000 atoms, >49,000 of which represent water molecules, plus the non-frozen residues at the protein-solvent interface (~8500 additional atoms).

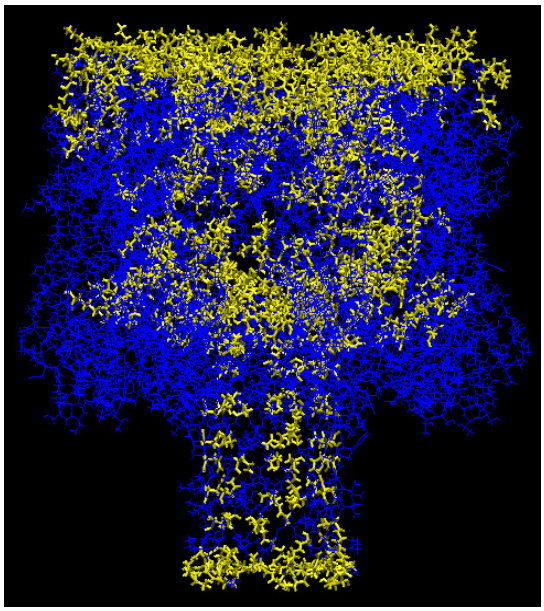

Figure 6. A picture showing the residues at the protein-solvent interface (yellow) that were selected to move during our current production runs. (Kowallis and Coalson, in progress) [0]

Calculations currently in progress consist of a concentration of 1M NaCl and an applied voltage range of -500 mV to +500 mV in order to replicate simulation conditions for the testing of voltage-current characteristics previously obtained via PNP. The main purpose in running long NEMD trajectories is to collect adequate statistical data about ion permeation events through the channel. Assuming that these events are independent of each other, the trajectory as a whole can be split up into smaller parts, e.g. a 10 ns trajectory (which would show about 25 permeation events for a current of 400pA) can be split up into 1 ns segments that can then be run concurrently. All output files were analyzed using the program Visual Molecular Dynamics, or VMD (Humphrey et al., 1996).

4.0 CALCULATIONS

4.1 CALCULATION OF ION CURRENTS

Current was calculated by counting the number of ions that pass through the pore during the trajectory output files. The number of charges passing through the pore per unit time can easily be converted into a current, conveniently expressed in picoamps. In narrower channels, the time of a permeation event is sometimes judged to be the amount of time for an ion to enter one side of the channel and for another ion, not necessarily the same one, to exit the other side (Cohen and Schulten, 2004). However, this may not be the most appropriate method for the α-HL system considering that: 1.) Its ions are not in a single file inside the channel. 2.) Ions are much more numerous inside the α-HL channel as compared to other well-studied ion channels (e.g. ClC, KcSA, GA). 3.) Ions are in exchange at either end of the channel – that is, a particular ion may enter and exit the pore opening several times before traversing the channel. Considering the structure of the pore, with a large vestibule in the cap domain and the narrow, more selective region in the stem domain, there is higher exchange between the vestibule and the cytosol than between the stem region and the periplasm. So, for this study, permeation events are counted as the passage of ions through the stem region of the pore. This is further supported by the fact that is it the stem domain of α-HL that actually spans the phospholipid bilayer (Fig. 3) and so corresponds to where the ions would physically traverse the bilayer.

4.2 DIFFUSION CONSTANT CALCULATION

According to various articles (Allen et al., 2004; Chui et al., 1993, Mamanov et al., 2003) as well as research currently underway in this group, there is a reduction in the diffusion constant (D) for ions in solution upon their entrance into an ion channel, dependent upon the channel properties, including pore radius. One proposed reduction is around 70% for the Gramicidin A channel (Allen et. al, 2004). We have calculated D for ions (at zero applied voltage) to see if this reduction is also apparent in α-HL. These calculations should also show that the value of D for sodium cation, the smaller of the two ions (0.85Å in rad. for Na+ compared to 1.50Å for Cl-), should be greater than D for chloride anion since diffusion is inversely proportional to the radius (R) of a spherical particle in solution, according to $\frac{k_B T}{6\pi\eta R} = D$, where η is the viscosity of the medium (Atkins and de Paula, 2002). Further, these calculations of D would provide justification for the diffusion constant value used in our group's PNP calculations of current-voltage characteristics in α-HL (Kowallis and Coalson, in preparation).

The average diffusion constants for each ion type, both inside and outside of the pore, were determined by calculating their mean square deviation (MSD), or $\langle r^2 \rangle$, over a trajectory, plotting the MSD versus time, and taking the accumulated slope of this plot to yield D according to $\langle r^2(t) \rangle = 6Dt$, the equation for diffusion in three dimensions (McQuarrie, 1976). The cutoffs for delimiting internal D values were at -48Å at +48Å along the z-coordinate of the system, which correspond to the ends of the α-HL structure.

4.3 SELECTIVITY AND RECTIFICATION

Many ion channels have selectivity toward a specific type of atom, or at least an affinity for either positive or negative ions. Such properties for α-HL can easily be monitored by taking a ratio between the number permeant events of each ion type during production runs at each voltage bias. Also, channels may have a tendency to allow electrodiffusion of ions in one direction as opposed to the opposite direction, i.e. rectification. The degree of rectification can be quantified by comparing currents obtained at positive and negative voltage potentials.

4.4 CONCENTRATION PROFILES

Concentration profiles provide a helpful tool in ion channel study since they give insight into the location of binding sites for ions within the pore (indicated by high concentrations, relative to the rest of the channel) as well as narrow or more selective pore regions (characterized by lower relative concentrations). We calculated the concentration histogram by first finding the number of ions present in slices of thickness 2Å along the z-axis of the entire length of the α-HL pore. Then, the concentration in each of these slices is obtained as:

$$c_{i,a} = \frac{\#\,atoms\ of\ type\ a}{V \times n_t} \tag{6}$$

The concentration in a given slice (i) for ion of type a ($c_{i,a}$), is equal to the sum of ions in that slice over the entire trajectory divided by the product of the slice volume (V) times the number of time steps (n_t) in the trajectory. Such profiles will be calculated at every voltage bias

for each ion type as we complete our production runs, with profiles for +200mV and +500mV from our preliminary calculations shown in the results section.

5.0 RESULTS

5.1 BENCHMARK ESTIMATES FOR NEMD CALCULATIONS USING NAMD

Information for benchmarking purposes was gathered during initial simulations on the Lemieux cluster, using our PSC development grant. We found that, for the α-HL system in our initial setup and equilibration, where approximately 51,600 atoms were free to move, the required computational power required to simulate under an NTP ensemble with a time step of 2fs was approximately 896 service units, or processor-hours, for 600,000 fs of simulation, operating on 32 nodes (128 processors) in parallel. This corresponds to approximately 1400 processor-hours required for the production of 1 ns simulation time. In production runs, where cell volume is fixed, and using a newer version of NAMD software and a time step of 3fs, we find that 512 processor-hours correspond to 450,000 fs of simulation, or approximately 1138 processor-hours for the production of 1 ns simulation time.

5.2 VOLTAGE-CURRENT CHARACTERISTICS

In data collected in simulations from grant #mcb030021p, we found that NEMD simulations of this system produces results that are qualitatively accurate (with respect to selectivity and rectification) in comparison to experimental data (Misakian and Kasianowicz, 2003) and

quantitatively similar (with respect to I-V data) to those produced through 3-D Poisson Nernst-Planck method (Kowallis and Coalson, in preparation). Specifically, both anion selectivity (at +200 mV) and inward rectification (through comparison to a short 4ns run at –200mV) were observed during production runs. The I-V results are summarized below (Table 1).

Table 1. I-V characteristics for α-HL in 1M NaCl. *Misakian and Kasianowicz, 2003.

Voltage	EXPT*	NEMD	PNP
+1 (for 10ns)	~	1450pA	800pA
+500 mV(for 12ns)	~	400pA	325pA
+200mV (for 6.5ns)	120pA	160pA	180pA
-200mV (for 5ns)	170pA	175pA	120pA

5.3 DIFFUSION CONSTANT CALCULATIONS

MSD values were computed at 0V applied potential for both sodium and chloride ions and were used to calculate diffusion constant values by plotting MSD versus time (Fig. 7), as explained in section **4.2**. A summary of the calculations is given below (Table 2).

Table 2. Diffusion values for ions in the α-HL system using MSD method.

Ion	External (Å^2/ps)	Internal (Å^2/ps)	Reduction (%)
Na+ at 0mV	0.11123722	0.050780744	54.3
Cl- at 0mV	0.079667711	0.03815911	52.1
		average	**53.2**

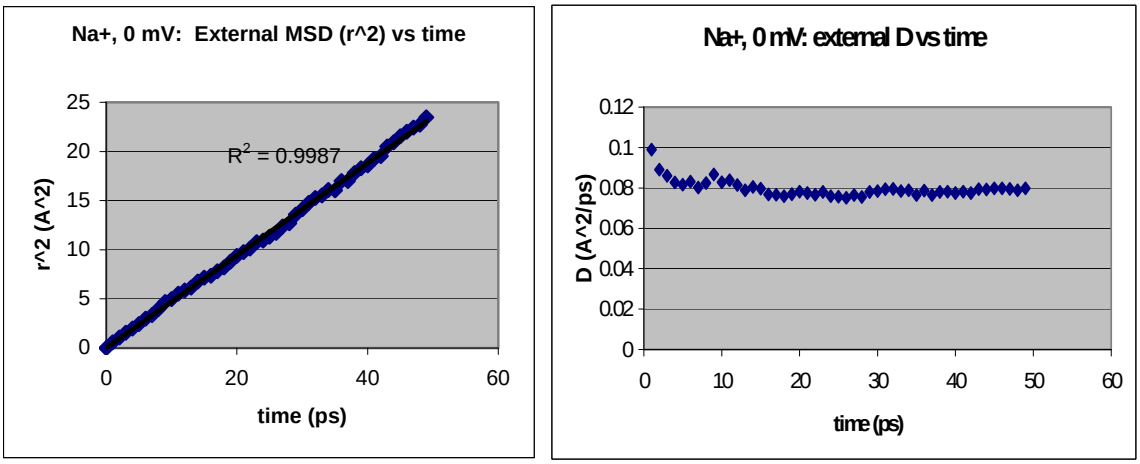

Avg. D(External Na+, 0mV) = 0.11123722

Figure 7. A sample plot for the calculation of D for ions in the simulation system. The above graphs are for Sodium cation at 0V applied potential. The left plot is mean squared displacement vs. time, while the right plot is a calculation of D as determined from the accumulated slope in the plot on the left.

5.4 ION SELECTIVITY

The selectivity of anions (Cl-) over cations (Na+) occurs in a 4:1 ratio in NEMD simulations at +200mV, which is slightly higher than the ratio predicted with PNP (1.5:1).

Interestingly, this trend is reversed for a bias of +1V, where Na+ permeates at a rate three times greater than Cl-. Apparently, at such a large voltage bias, the energy required to pass through the selectivity filter is effectively negated; in addition, Na+ cations are much smaller (0.85Å in rad.) than Cl- anions (1.50Å). Calculating the electric potential profile along the length of the channel would further elucidate these mechanistic issues.

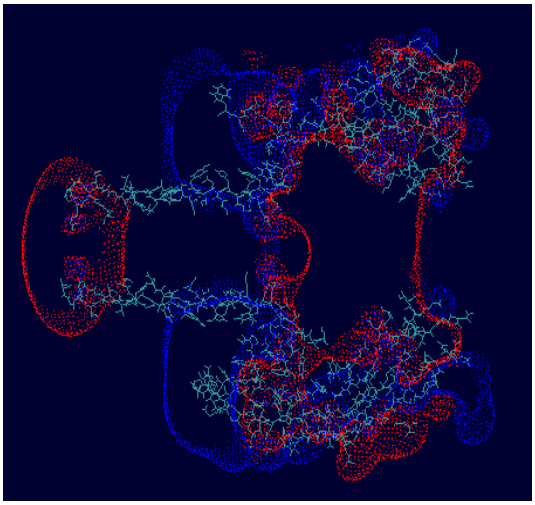

Figure 8. Charge profile of α-HL structure. Red represents negative charge while blue represents positive charge. (Kowallis and Coalson, in preparation).

5.5 CONCENTRATION PROFILES

The concentration profiles are given in values of millimolar concentration for both Na+ and Cl- ions (Figs. 9-12). The concentration profiles for both +200 mV (Fig. 9) and +500 mV (Fig. 11) were characterized by considerable scatter in concentrations at a few distinct points over the

length of the channel. Upon inspection of the trajectory files, we found that ions at some points in the channel structure had become suck by migrating into the [frozen] pore structure and were unable to move from these locations over the entire course of the trajectory, most likely due to the fact that the atoms along these pore residues were not vibrating. This issue is discussed further in section **6.2**. When these stuck ions were excluded from the calculations for the concentrations, the profile showed a more continuous change in concentrations (Figs. 10, 12).

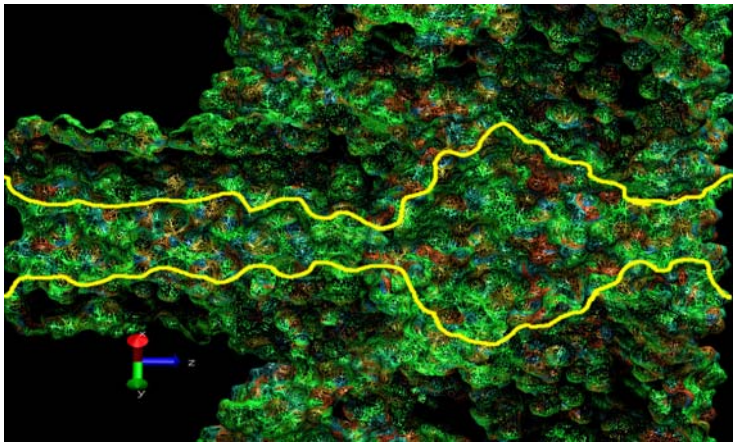

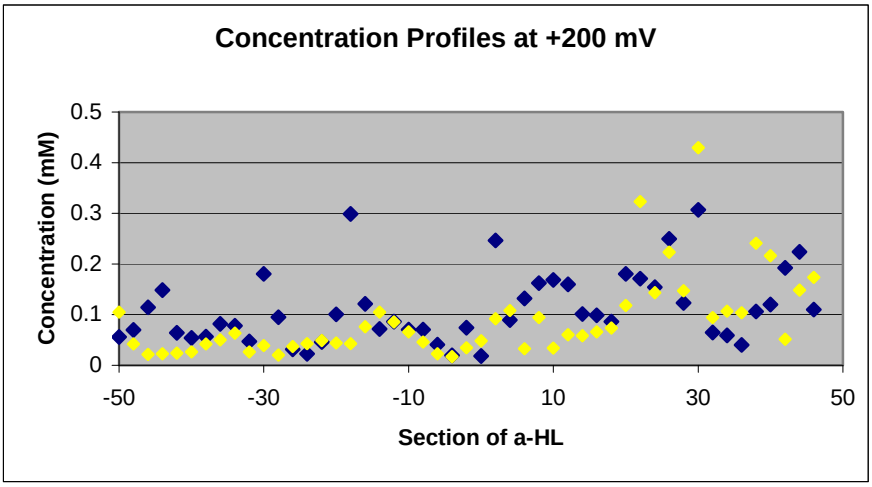

Figure 9. The top figure is of α-HL with the pore [approximately] outlined, extracellular space to the left and intracellular to the right. Charges in the structure are represented as follows: green = neutral, red = negative, blue = positive. The bottom figure is concentration profile at +200 mV for 4ns of simulation; Cl- are shown as blue dots and Na+ are Yellow. Note that the concentrations are, in general, lower for Na+ than Cl-; also, the concentration in the vestibule is higher than in the narrow, more selective part of the channel. In general, high concentration values in Cl- concentrations reflect areas of positive charge (blue) along the pore surface; likewise, high concentration points in Na+ correspond to regions of high negative potential along the pore surface. (Kowallis and Coalson, in progress) [0]

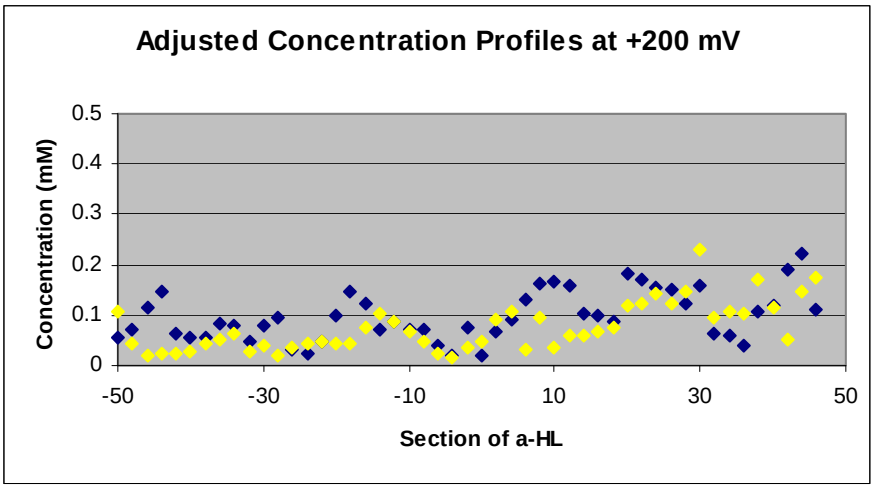

Figure 10. A Concentration profile for the same trajectory as Fig. 9, but here, ions that became stuck in the frozen α-HL pore structure were excluded from the calcu-lations. (Kowallis and Coalson, in progress)[0].

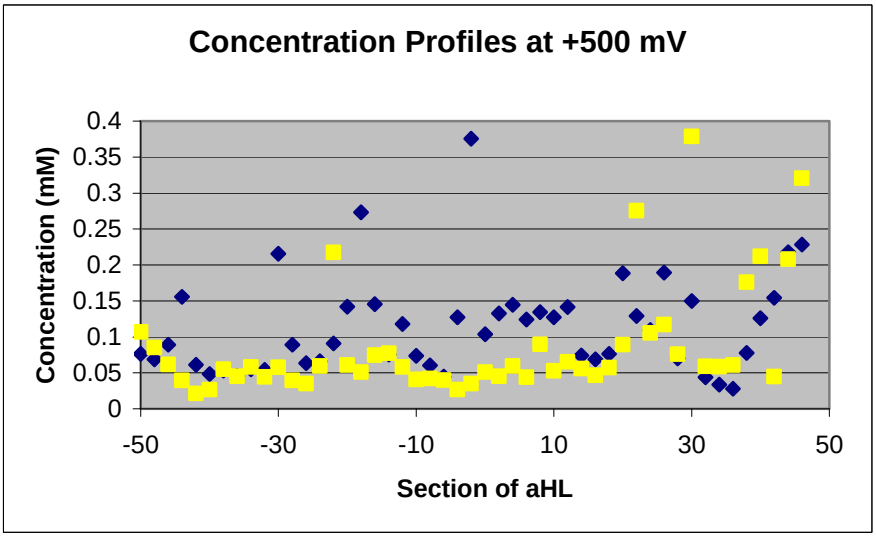

Figure 11. A Concentration profile of α-HL at +500 mV over a 12ns trajectory. Blue and yellow dots represent chloride and sodium ion concentrations, respectively. (Kowallis and Coalson, in progress)[0].

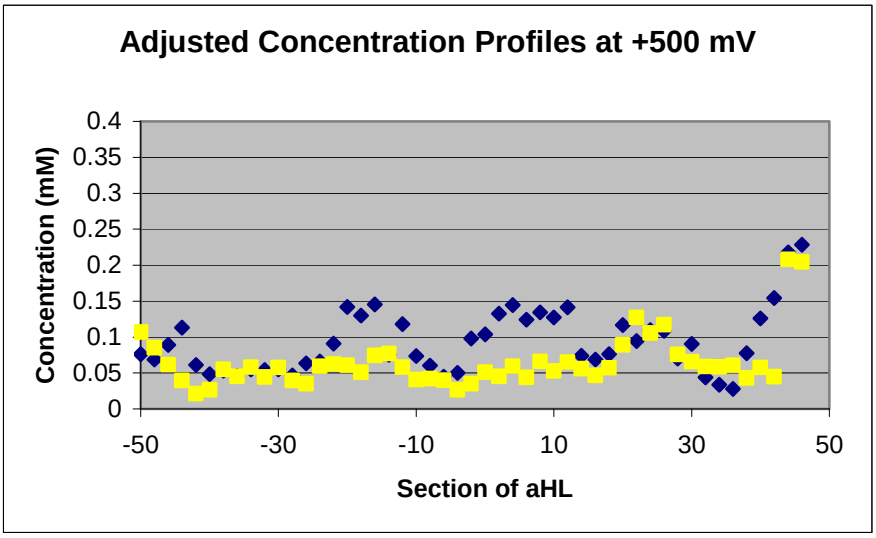

Figure 12. A Concentration profile for the same trajectory as Fig. 11, again, ions that became stuck in the frozen α-HL pore structure were excluded from the calcu-lations. A much smoother profile is produced. (Kowallis and Coalson, in progress)[0].

6.0 RESULTS

6.1 JUSTIFICATION FOR USING DUMMY ATOMS IN PLACE OF A SIMULATED MEMBRANE MEMBRANE AND FOR FREEZING THE PORE STRUCTURE

Clearly, the most realistic simulation setup would have the protein embedded in a membrane with all atoms, both in the protein and bilayer, free to move. However, especially in the case of a large protein such as α-HL, large-scale motions, which result in changes in the overall shape of the channel structure, e.g. breathing, would not be accounted for on the nanosecond time scale of these simulations. Considering this, the lipid bilayer can be substituted be substituted by frozen L-J spheres and the α-HL structure partially or entirely frozen, thereby vastly decreasing the required amount of simulation time for these computations.

6.2 JUSTIFICATION FOR FREEING RESIDUES AT THE PROTEIN-SOLVENT INTERFACE IN CURRENT STUDIES

Freeing residues at the protein surface to allow for their motion during production runs serves to increase the realism of the system in a number of ways. First, the motion of the residues at the pore-lining changes the size and shape of the pore itself. Also, the amino acids found lining the pore surface would have the highest impact in altering the electrostatic potential inside of the

pore. Finally, most of the charged and polar groups in the protein structure are found at the protein (esp. pore) surface. These are the residues that have the largest influence on permeation due to their effect on pore volume as well as their effect on electrostatic potentials inside the channel. In addition, freeing these residues near the pore surface reduces the likelihood that an ion will get stuck at one place in the structure, as noted above in the concentration profiles (Figs. 9-12), since the fluctuations of these amino acids will eliminate the constant gaps in the frozen pore structure that allow ions to become lodged in the α-HL structure.

6.3 ADVANTAGES OF USING A SIMULATED PHOSPHOLIPID BILAYER

The simulation setup for this set of calculations had α-HL almost entirely surrounded by a layer of L-J spheres (Fig. 5), whereas in a realistic scenario, just the stem domain and part of the rim domain are embedded in a phospholipid bilayer (Fig. 3). One factor of interest here is that amino acids on the outer cap region do not have the ability to interact with solvent in our current simulation setup since they are covered by the layer of L-J spheres, whereas their interaction with real solvent, especially the titratable groups, may influence the electrostatic potential inside the channel (Kowallis and Coalson, in preparation).

6.4 DIFFUSION CONSTANT CALCULATION RESULTS

As can be seen in Table 2, the results produced via MSD calculation of diffusion constant values show a reduction of approximately 50% upon an ion's entrance into the α-HL channel. While

there is no experimental data with which to compare these results for our simulation system, it may serve as useful information when applying diffusion constant values in other computation methods, e.g. PNP and BD.

Another consideration with regards to this system is that D may vary according to the diameter of a given channel. Specifically, α-HL has a pore with a wide vestibule (~45Å in dia.) and a narrower region (~15Å in dia.), D can be measured for each of these areas, using z-coordinate boundaries of +48Å to -1Å for the vestibule and -1Å to -48Å for the stem region. We will use the MSD method to extract D for both sodium and chloride ions in each of these regions. Further calculations of diffusion constants via other means such as force autocorrelation function (FACF) (Mamanov et al., 2003) and velocity autocorrelation function (VACF) (Allen et al., 2004) will be performed in order to verify our results obtained via the MSD method.

6.5 CURRENT-VOLTAGE RESULTS

The current-voltage results show that, using the charge set given in the crystallographic data and CHARMM27, the I-V data from our preliminary studies (where the entire pore structure was fixed) compare well with experimental data (Table 1). The value in current for –200mV was obtained after only 4ns of production runs, and thus will be recalculated again after further simulation. Consistent with experimental data (Misakian and Kasianowicz, 2003), inward rectification is noted for our simulation system – that is, calculated current at –200mV is greater in magnitude than current calculated at +200mV. One parameter that may need to be further adjusted in the charge set is that titratable groups within the α-HL may have average charges different than those given by CHARMM27 (Kowallis and Coalson, in preparation). This is

further supported by finding that PNP simulations of α-HL were markedly more accurate compared to experimental results when the charges on titratable amino acids in the structure were adjusted (ibid).

6.6 FUTURE APPLICATIONS

The results of this simulation method thus far have shown that NEMD method is a viable option for voltage-current calculation of some types of ion channels, particularly those in which the time required for a permeation event is sufficiently small to allow for data to be collected at least on the order of tens of events. This simulation served as a staring point to be applied to other systems of greater biological interest, particularly smaller channels such as KcSA and KvAP, which are both potassium channels with minimum pore dia. of ~4-5Å, ClC, which is a chloride channel with a min. pore dia. of ~5Å, as well as Glycine Receptor and NAChR, which both have minimum dia. of ~6Å. Also, while it appears to be sufficient to allow α-HL to be embedded in dummy atoms for this simulation, it is important to include a more realistic membrane in future work dealing with these channels considering that small protein fluctuations and subtle differences in electric potential inside the channel have a much more significant effect as the pore becomes narrower. Possibilities for a more realistic membrane include using a fully atomistic phospholipid bilayer, e.g. dimyristoylphosphatidylcholine (DMPC), or using coarse grain model (Shelley et al., 2001) in order to reduce computational load, where both the charged head group as well the lipid sections of the membrane are represented as large spheres.

BIBLIOGRAPHY

Alder, B.J. and T.E. Wainwright. 1957. Phase transition for a hard sphere system. *Journal of Chemical Physics*, **27**, 1208-1209.

Alder, B.J. and T.E. Wainwright. 1959. Studies in Molecular Dynamics I. General Method. *Journal of Chemical Physics*, **31 (2)**, 459-466.

Allen, T.W., O.S. Anderson, B. Roux. 2004. Energetics of ion conduction through the gramicidin channel. *Proc. Nat. Acad. Sci USA* **101**, 117-122.

Atkins P. and de Paula, J. 2002. Physical Chemistry. Oxford University Press. p. 742.

Barcilon, V., D. Chen, R.S. Eisenberg, M.A. Ratner. 1993. Barrier crossing with concentration boundary conditions in biological channels and chemical reactions. *J. Chem. Phys.* **98**: 1193-1212.

Berendsen, H. J. C., J. P. M. Postma, W. van Gunsteren, A. DiNola, J.R. Haak. 1984. Molecular dynamics with coupling to an external bath. *J. Chem. Phys.*, **81**, 3684-3690.

Bernstein, F. C., T. F. Koetzle, G. J. Williams, E. F. Meyer, M. D. Brice, J. R. Rogers, O. Kennard, T. Shimanouchi, and M. Tasumi. 1977. The Protein Data Bank: a computer-based archival file for macromolecular structures. *J. Mol. Biol.* **112,** 535–542.

Bezrukov, S.M. and J.J. Kasianowicz. 1993. Current noise reveals protonation kinetics and number of ionizable sites in an open protein ion channel. *Phys. Rev. Lett.* **70**: 2352-2355.

Braha, O., B. Walker, S. Cheley, J.J. Kasianowicz, M.R. Hobaugh, L Song, J.E. Gouaux, H. Bayley. 1997. Structure-based design of a heteromeric transmembrane pore. *Chemistry & Biology* **4**: 497-505.

Brünger, A. T. 1992. X-PLOR, Version 3.1: A System for X-Ray Crystallography and NMR. The Howard Hughes Medical Institute and Department of Molecular Biophysics and Biochemistry, Yale University Press.

Chen, D.P., V. Barcilon, R.S. Eisenberg. 1992. Constant fields and constant gradients in open ionic channels. *Biophys. J.* **72**: 1372-1393.

Chen, D.P. and R.S. Eisenberg. 1993. Charges, currents, and potentials in ionic channels of one conformation. *Biophys J.* **64**: 1405-1421.

Chiu S. W., J. A. Novotny, E. Jakobsson. 1993. The nature of ion and water barrier crossings in a simulated ion channel, *Biophys. J*. **64**(1) 98-108

Chung, S.H., M. Hoyles, T. Allen, and S. Kuyucak. 1998. Study of ion currents across a model membrane channel using Brownian dynamics. *Biophys J.* **75**: 793-809.

Cohen, J, and K. Schulten. 2004. Mechanism of Anionic Conduction Across ClC. *Biophysical Journal*, **86**, 836-845.

Cooper, K.E., E. Jakobsson, P. Wolynes. 1985. The theory of ion transport through membrane channels. *Prog. Biophys. Mol. Biol.* **46**: 51-96.

Corry, B., S. Kuyucak, and S.H. Chung. 2000. Tests of continuum theories as models of ion channels. II. Poisson-Nernst-Planck theory versus Brownian Dynamics. *Biophys J.* **78**: 2364-2381.

Crozier, Paul. S., D. Henderson, R. L. Rowley, D. D. Busath. 2001. Model Channel Ion Currents in NaCl-Extended Simple Point Charge Water Solution with Applied-Field Molecular Dynamics. *Biophys J.* **81**: 3077-3089.

Crozier, P.S., R.L. Rowley, N.B. Holladay, D. Henderson, and D.D. Busath. 2001. Molecular Dynamics Simulation of Continuous Current Flow Through a Model Biological Membrane Channel. *Phys. Rev. Lett.* **86**, 2467.

Darden, T., D. York, and L. Pedersen. 1993. Particle Mesh Ewald. An N_log(N) method for Ewald sums in large systems. *J. Chem. Phys.* **98**, 10089–10092.

Doyle DA, C.J. Morais, R.A. Pfuetzner, A. Kuo, J.M. Gulbis, S.L. Cohen, B.T. Chait, R. MacKinnon. 1998. The structure of the potassium channel: molecular basis of K+ conduction and selectivity. *Science.* **280**, 69-77.

Dutzler, R, E. B. Campbell, M. Cadene, B. T. Chait, & R. MacKinnon. 2002. X-ray structure of a ClC chloride channel at 3.0 Å reveals the molecular basis of anion selectivity. *Nature.* **415**, 287-294.

Dutzler, R., E. B. Campbell, M. Cadene, and R. MacKinnon. 2003. Gating the selectivity filter in ClC chloride channels. *Science.* **300**: 108-12.

Eisenberg, R.S., M.M. Klosek, Z. Schuss. 1995. Diffusion as a chemical reaction: Stochastic Trajectories between fixed concentrations. *J. Chem. Phys.* **102**: 1767-1780.

Feller, S. E., Y. H. Zhang, R. W. Pastor, and B. R. Brooks. 1995. Constant pressure molecular dynamics simulation—the Langevin piston method. *J. Chem. Phys.* **103,** 4613–4621.

Feller, S. E., and A. MacKerell. 2000. An improved empirical potential energy function for molecular simulations of phospholipids. *J. Phys. Chem. B.* **104**, 7510–7515.

Ford, J. 1973. The Transition from Analytic Dynamics to Statistical Mechanics. *Adv. Chem. Phys.* **24**, 155-158.

Gouaux, J.E., O. Braha, M.R. Hobaugh, L.Z. Song, S. Cheley, C. Shustak, H. Bayley. 1994. Stochastic Stoichiometry of Staphylococcal alpha-hemolysin in crystals and on membranes – a heptameric transmembrane pore. *Proc. Natl. Acad. Sci.* **91**: 12828-12931.

Gouaux, J.E. 1998. α-hemolysin from *Staphylococcus aureus*: An archetype of β-barrel, channel-forming toxins. *J. Struct. Biol.* **121**: 110-122.

Graf, P., A. Nitzan, M. G. Kurnikova, and R. D. Coalson. 2000. A dynamic lattice Monte Carlo model of ion transport in inhomogeneous dielectric environments: Method and implementation. *J. Phys. Chem. B* **104**: 12324-12338; P. Graf, M. G. Kurnikova, R. D. Coalson and A. Nitzan, "Comparison of Dynamic Lattice Monte-Carlo Simulations and Dielectric Self Energy Poisson-Nernst-Planck Continuum Theory for Model Ion Channels", *J. Phys. Chem. B*, in press (10/03).

Grubmüller, H. 1996. SOLVATE 1.0. http://www.mpibpc.gwdg.de/abteilungen/071/solvate/docu.html.

Henderson, D., D.D. Busath, R.L. Rowley, P.S. Crozier, and D. Boda, 2001. Simulation study of channels in biological membranes. *Proceedings of the International Conference on Computaional Nanoscience*, pp. 45-48.

Hoover, W. G. 1985. *Phys. Rev. A*, **31**, 1695.

Humphrey, W., A. Dalke, and K. Schulten. 1996. VMD—visual molecular dynamics. *J. Mol. Graph.* **14**, 33–38.

Jordan, P.C. 1982. Electrostatic modeling of ion pores. Energy barriers and electric field profiles. *Biophys. J.* **39**: 157-164.

Jordan, P.C. 1983. Electrostatic modeling of ion pores. II. Effects attributable to the membrane dipole potential profile. *Biophys. J.* **41**: 189-195.

Jordan, P.C. 1984. Effect of pore structure on energy barriers and applied voltage profiles. I. Symmetrical channels. *Biophys. J.* **45:** 1091-1100.

Jordan, P.C. 1984 . Effect of pore structure on energy barriers and applied voltage profiles. II. Unsymmetrical channels. *Biophys J.* **45**: 1101-1107.

Jordan, P.C. 1987. Microscopic approaches to ion transport through transmembrane channels. The model system gramicidin. *J. Phys. Chem.* **91**: 6582-6591.

Kale, L., R. Skeel, M. Bhandarkar, R. Brunner, A. Gursoy, N. Krawetz, J. Phillips, A. Shinozaki, K. Varadarajan, and K. Schulten. 1999. NAMD2: Greater scalability for parallel molecular dynamics. *Journal of Computational Physics* **151**: 283-312.

Kumar, S., D. Bouzida, R. H. Swendsen, P. A. Kollman, & J. M. Rosenberg, 1992. Molecular dynamics simulations suggest that the Eco RI kink is an example of molecular strain. *J. Comp. Chem.* **13**, 1011-1021.

Kasianowicz, J.J., S.M. Bezrukov. 1995. Protonation dynamics of the α-toxin ion channel from spectral analysis of pH dependent current fluctuations. *Biophys. J.* **69**: 94-105.

Kurnikova, M. G, R. D. Coalson, P. Graf, & A. Nitzan. 1999. A lattice relaxation algorithm for three-dimensional Poisson-Nernst-Planck theory with application to ion transport through the gramicidin A channel. *Biophys. J.* **76**, 642-656.

Kwack P., R. D. Coalson. In preparation. Ion permeation through Alpha-Hemolysin channel studied by three-dimensional Poisson Nernst-Planck Theory.
Levitt, D.G. 1999. Modeling ion channels. *J. Gen. Physiol.* **113**: 789-794.

Mamonov, A., R. D. Coalson, A. Nitzan and M. G. Kurnikova. 2003.The Role of the Dielectric Barrier in Narrow Biological Channels: a Novel Composite Approach to Modeling Single Channel Currents, *Biophys. J.* **84**(6): 3646-3661

McCammon, J.A., Gelin, B.R., Karplus, M. 1977. *Nature (London)*, **267**, 585.

McQuarrie, D.A. 1976. Statistical Mechanics. Harper Collins Publishers, New York. p. 514.
Menestrina, G. 1986. Ionic channels formed by *Staphylococcus aureus* alpha-toxin: Voltage-dependent inhibition by divalent and trivalent cations. *J. Membr. Biol.* **90**: 177-190.

Miller, C. 1982. Open-State Substructure of Single Chloride Channels from Torpedo Electroplax. *Phil. Trans. Roy. Soc. Lon. B.* **299**, 401-411.

Misakian M. and J. J. Kasianowicz. 2003. Electrostatic control of ion transport through the α-hemolysin channel. *Journal of Membrane Biology,* **195 (3)**, 137-146.

Neher, E and B. Sakmann. 1976. Noise analysis of drug induced voltage clamp currents in denervated frog muscle fibres. *The Journal of Physiology*, **258 (3)**, 705-729.

Nose, S. 1984. A unified formulation of the constant temperature molecular dynamic method. *J. Chem. Phys.*, **81**, 511-519.

Rahman, A. 1964. *Correlations in the Motion of Atoms in Liquid Argon.* Physical Review A*, **136**, 405-411.*

Shelley, J. C., M. Y. Shelley, R. C. Reeder, S. Bandyopadhyay, M. L. Klein. 2001. A Coarse Grain Model for Phospholipid Simulations. *J. Phys. Chem. B,* **105**, 4464-4470.

Schlenkrich, M., J. Brickmann, A. D. MacKerell, Jr., and M. Karplus. 1996. Empirical potential energy function for phospholipids: criteria for parameter optimization and applications. In Biological Membranes: A Molecular Perspective from Computation and Experiment. K. M. Merz, and B. Roux, editors. Birkhauser, Boston, MA. 31–81.

Song, L., M. R. Hobauch, C. Shustak, S. Cheley, H. Bayley, and J. E. Gouaux. 1996. Structure of Staphlococcal alpha-hemolysin, a heptameric transmembrane pore. *Science*, **274**, 1859-1866.

Stillinger, F.H., Rahman, A. 1974. *Journal of Chemical Physics*, **60**, 1545.

Swope, W.C.; Andersen, H.C.; Berens, P.H.; and Wilson, K.R. 1982. A computer simulation method for the calculation of equilibrium constants for the formation of physical clusters of molecules: Application to small water clusters. *J. Chem. Phys.* **76**, 637

Torrie, G. M. & J. P. Valleau. 1977. Nonphysical sampling distributions in Monte Carlo free energy estimation: Umbrella sampling. *J. Comp. Phys.* **23**, 187-199.

van Gunsteren, W.F. and Berendsen, H.J.C. 1977. Algorithms for macromolecular dynamics and constraint dynamics. *Mol. Phys.*, **34**: 1311-1327.

Windhover's Review of Emerging Medical Ventures 2003. The reemergence of Ion Channel Drug Discovery. **8(5)**, p. 9.

Wymore, T.; Deerfield II, D.W.; Field, M.J.; Nicholas, H.B.; Hempel, J. 2002. Initial Events in class 3 Aldehyde Dehydrogenase: MM and QM/MM simulations. *Chemico-Biological Interaction*s, **130**, 201-207.